Numerical Investigation of a Silicon Six-Wafer Microcombustor Under the Effect of Heat Loss Through the Outer Walls

Lin Zhu
School of Engineering,
Anhui Agricultural University,
Hefei 230036, P.R. China;
Department of Mechanical Engineering,
University of Wisconsin,
Milwaukee, WI 53211
e-mail: zl009@mail.ustc.edu.cn

Tien-Chien Jen
Department of Mechanical Engineering,
University of Wisconsin,
Milwaukee, WI 53211
e-mail: jent@uwm.edu

Xiao-Ling Kong
School of Engineering,
Anhui Agricultural University,
Hefei 230036,
P.R. China
e-mail: kong923@126.com

In this paper, the influences of low heat transfer condition at the outer walls on the microcombustor are investigated due to the fact that a sufficiently small heat transfer coefficient at the outer wall incurs the upstream burning in the recirculation jacket, results in the high wall temperature, and hence possibly damages the microcombustor. Numerical simulation approaches focused on the microcombustor with the flame burning in the recirculation jacket. Combustion characteristics of the combustor were first analyzed based on 2D computational fluid dynamics (CFD), and then the most dangerous locations on the combustor were predicted by means of the 3D finite element analysis method. The study demonstrates the effectiveness of CFD and stress modeling for the design and improvement of the microcombustors.
[DOI: 10.1115/1.4002804]

1 Introduction

With the rapid development of various kinds of miniature devices such as notebook computers, mobile phones, walking robots, etc., the availability of compact, highly mobile, and efficient micropower supply systems is becoming increasingly important in our daily lives. Currently, most of these devices are powered by batteries. They can only continuously work for a certain period of time so that they may need recharging frequently [1–6]. Therefore, a lightweight and high power density micropower source is greatly demanded to improve our quality of life. A combustion-based microgas turbine engine is one of the most promising micropower sources due to its higher power density, smaller volume, and less pollution than any other type of micropower sources, e.g., microfuel cells, etc. [2].

The MIT group has studied the combustion behavior in a standalone microcombustor without the rotating parts of the microcompressor and microturbine. The results show that [3] the combustion could occur within the combustion chamber under certain designed operating conditions in the laboratory. However, under more realistic application conditions, the performance of the combustor may be affected by factors such as loading variation, environmental condition changes, etc. It is observed [2–4] that the flame burns in the recirculation jacket of the microgas turbine engine under lower outer wall heat loss conditions. Consequently, the combustor wall temperature could be higher than the upper limit of the material's allowable temperature, resulting in a short lifetime of the combustor. It is well known that the microcombustor from MIT is made of silicon, and that the adiabatic flame temperature of premixed stoichiometric mixture can reach as high as 2400 K [3]. Sufficient high temperature causes the yield strength of silicon to drop off rapidly and hence the transitions from a brittle to a plastic material and creep failure when the temperature is above 900 K [7]. Therefore, it is very critical to investigate the effects of heat loss through the outer walls on the microcombustor device. To the best of our knowledge, no research publication is available on the effects of the different operation conditions on the microcombustor device. This research is aimed to fill this gap.

In this study, the influences of the heat transfer condition at the outer wall on the microcombustor are investigated. The most dangerous locations on the combustor are predicted using a numerical simulation based on explicit CFD and finite element analysis (FEA) software.

2 CFD Model and Simulation Approach

2.1 Model Geometry. Based on Refs. [2,3], the geometry of the 2D microcombustor in this study was constructed in GAMBIT using the frame modeling method (see Fig. 1). The modeled combustor consists of the important static components of the microgas turbine engine, including recirculation jacket, flame holder, combustion chamber, and stators of compressor and turbine. Since the combustion characteristics of the combustor were the primary objective of this study, the rotating parts of compressor and turbine and the fuel injector in this model were not considered.

2.2 CFD Modeling. Figure 2 shows the meshed CFD model of the microcombustor. The CFD model includes the hydrogen/air flow path, the combustion chamber, and the conjugated heat transfer in solid engine walls. Commercial CFD software FLUENT 6.0 was used to perform the numerical analyses on fluid flow, heat transfer, and the chemical reactions in the microcombustor.

As distinguished from Ref. [2], CHEMKIN models in FLUENT

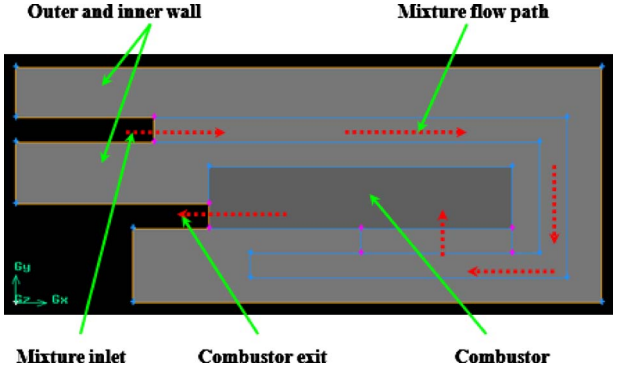

Fig. 1 Schematic of half of the axisymmetric six-wafer microcombustor

Contributed by the Design Innovation and Devices of ASME for publication in the JOURNAL OF MECHANICAL DESIGN. Manuscript received November 4, 2009; final manuscript received October 12, 2010; published online November 23, 2010. Assoc. Editor: Alexander Slocum.

 Copyright © 2010 by ASME

Downloaded From: http://asmedigitalcollection.asme.org/ on 10/11/2015 Terms of Use: http://www.asme.org/about-asme/terms-of-use

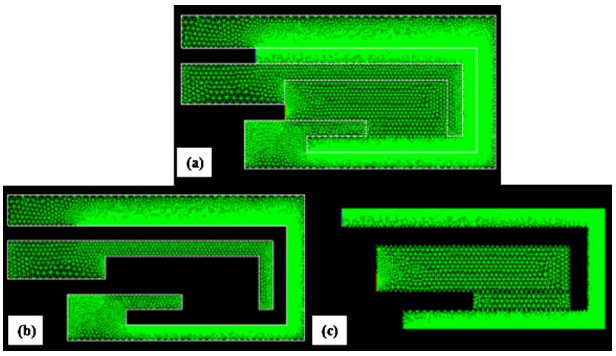

Fig. 2 (*a*) Total CFD mesh, (*b*) CFD mesh for heat exchange area, and (*c*) CFD mesh for flow and combustion area

6.0 were utilized to express the detailed chemical kinetics of hydrogen/air combustion. The gas phase mechanisms are similar to those in Refs. [2,8].

For all simulation cases, the inlet temperature of the mixture was assumed to be 300 K, a fixed pressure of 1.01325×10^5 Pa was specified at the combustion chamber outlet, and a no-slip boundary condition, as well as a no species flux normal to the wall surface, was applied at the wall. The convective and radiative heat losses to the ambient at the external wall were also considered. For simplicity, constant convective heat transfer coefficient and radiative emissivity were assumed at the outer wall. Additionally, the thermal conductivity of the combustor wall was assumed to have a constant value at 149 W/m K.

3 Results and Discussions

In order to compare the calculated results in this paper with Ref. [2], the corresponding parameters were chosen as follows:

- $h=50,150,250$ W/m^2 k
- $V=0.2$ g/s, $\varepsilon=0.85$, $\delta=0.5$

The temperature distributions of the microcombustor under the various heat transfer coefficients are presented in Fig. 3. Also, the calculated results from Ref. [2] are shown in Table 1 and Fig. 4.

As seen from Figs. 3(*a*) and 4, the upstream burning occurs in the recirculation jacket when the heat transfer coefficient at the outer wall equals to 50 W/m^2 K, and the wall temperature near the flame is approximately 1200 K. This demonstrates that the obtained results are valid. Due to the high thermal conductivity of silicon, the heat transfer through the outside wall plays a significant role in heat removal from the combustor and hence is responsible for the lifetime of the combustor.

However, comparing Fig. 3 with Fig. 4 and Table 1, there exist some minor discrepancies, in particular, on the magnitude of the temperature and the distribution of the flame burning in the recirculation jacket. This may primarily be due to the different calculated models and the distinct approaches expressing the detailed chemical kinetics of mixture combustion.

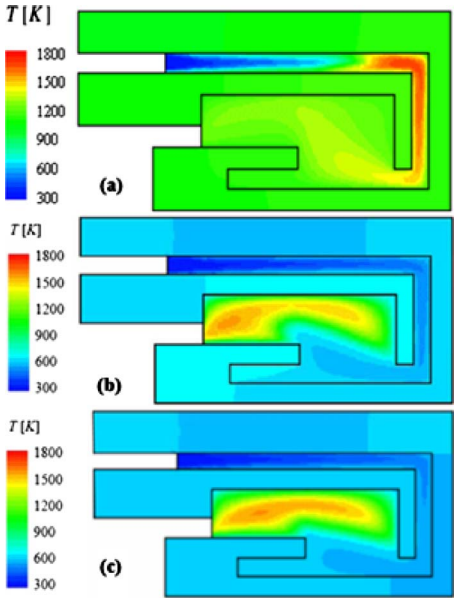

Fig. 3 Temperature distributions on the microcombustor with different heat transfer coefficients: (*a*) 50 W/m^2 K, (*b*) 150 W/m^2 K, and (c) 250 W/m^2 K

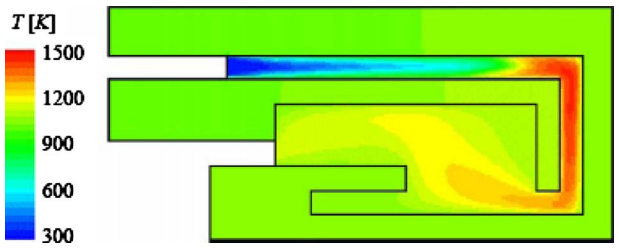

Fig. 4 Temperature distributions on the cross section of the microcombustor at heat transfer coefficients=50 W/m^2 K [2]

4 Structural Analysis

The fracture strength of silicon under the room temperature is extremely sensitive to the surface processing method [9], and also, the order of magnitude of thermal stresses can be as high as the available material yield strength if the structural temperature and temperature gradient are sufficiently high [7,10–14]. All of these have deleterious effects on the microcombustor device. Therefore, it is very critical and imperative to investigate on the structure of the microcombustor.

4.1 Analysis on Fabrication Process of the Microcombustor. Normally, bonding tool effects among the bonding issues are the most deleterious during fabricating the microcombustor. The postmortem analysis in the experiments indi-

Table 1 Calculated temperature and efficiency for different heat transfer coefficient conditions [2]

Heat transfer coefficient (W/m^2 K)	Flame temperature (K)	Exit gas temperature (K)	Outer wall temperature (K)	Efficiency (%)
50	1601	1192	1126	61
100	1695	1356	727	80
150	1666	1318	672	77
200	1642	1288	628	75
250	1622	1264	592	73
300	1606	1245	561	72

Downloaded From: http://asmedigitalcollection.asme.org/ on 10/11/2015 Terms of Use: http://www.asme.org/about-asme/terms-of-use

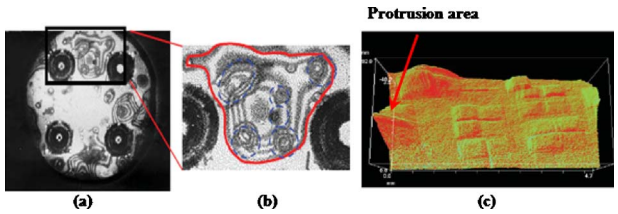

Fig. 5 (*a*) **Infrared image of five-wafer stack,** (*b*) **close-up view of a protrusion, and** (*c*) **surface image of the propagated defects** [10]

cated that the source of the defects was located at the interface between wafers 3 and 4, and that the defects created protrusions on the surface of the fourth wafer that was to be bonded to the subsequent fifth wafer (see Fig. 5).

4.2 Analysis on the Structure of the Microcombustor. When the heat loss through the outer wall is sufficiently low, the flame front could cause the wall temperature near the flame significantly high, incurring the wall distortion. This may further aggravate the effects of bow and warpage on the wafers, especially on the interfaces between wafers 3, 4, and 5. Consequently, this study focuses on thermal stress and strain analysis on the structure at high temperatures.

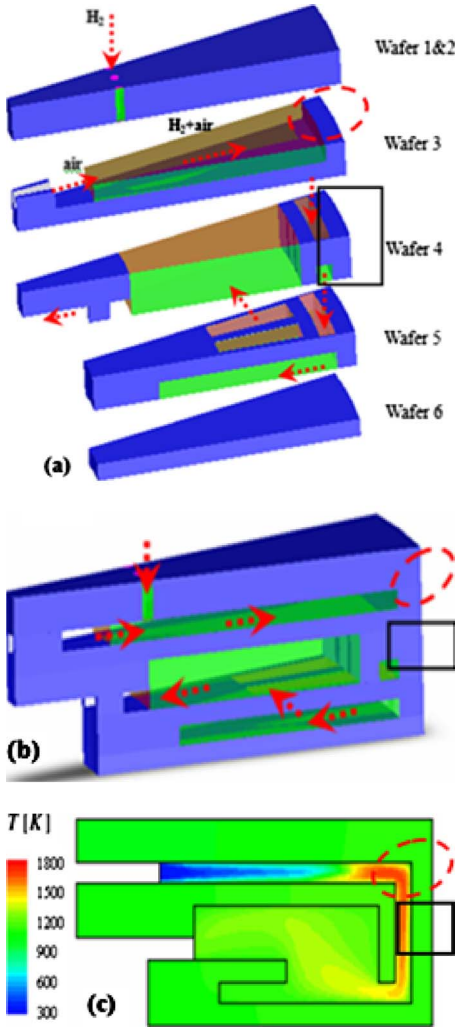

Fig. 6 Flow of the mixture in (*a*) **an exploded view,** (*b*) **an unexploded view, and** (*c*) **temperature distribution on the microcombustor with upstream burning in the recirculation jacket**

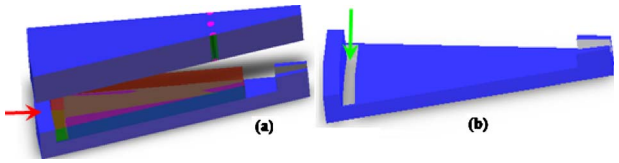

Fig. 7 Schematic of (*a*) **wafers 1, 2, and 3 and** (*b*) **wafer 3**

To make the problem tractable [10–14], three important assumptions are made:

- to neglect the high temperature oxidation results of silicon
- to ignore residual stress from the fabrication process of the combustor
- to emphasize the creep result of silicon due to the high temperature above 900 K

From Fig. 6, the creep failure may occur at the two locations of the combustor with flame burning in the recirculation jacket. The first location may be located at the interface of wafers 1, 2, and 3 (see the black dashed ellipse) because there are sharp angles where the stress could be congregated enough to promote creep failure easily by a large periodic thermal power input. The other may be located at the interface of wafers 3 and 4 based on Ref. [9]. Due to the large periodic thermal power inputs, the protrusions on wafer 4 could become larger than before, resulting in a poor bonding strength and failure.

4.3 Finite Element Analysis on Wafers 1, 2, and 3. For Fig. 7, the failure location at the junction of wafers 1, 2, and 3 was actually at the bonded position between the tail of wafer 3 and wafers 1 and 2 (see the red arrowhead). This is basically due to the fact that significantly high temperatures on the outer wall can increase the deleterious effects on bow and warpage. The FEM analysis focused on the tail of wafer 3 (see Fig. 7(*b*)).

The material used for the combustor was single crystal silicon, whose physical properties are [7] as follows:

- $EX=1.69\times10^{11}$ Pa, $\mu=0.28$, $\rho=2300$ kg/m^3, $\sigma_s=50$ MPa
- $C_p=700$ J/kg K, $K=32$ W/m K, $\alpha=10^{-6}$/K, $h=300$ W/m^2 K

It can be seen from Figs. 8 and 9 that the maximum stress and strain both occur at the interface of wafers 1, 2, and 3, i.e., the bonded location of wafers 1, 2, and 3. Consequently, under the combined effects of the congregated stress, the poor bonding, and the highest thermal stress and strain, the failure may occur at the interface of wafers 1, 2, and 3.

4.4 Finite Element Analysis on Wafers 3 and 4. Similarly, the failure location at the interface of wafers 3 and 4 may lie at the

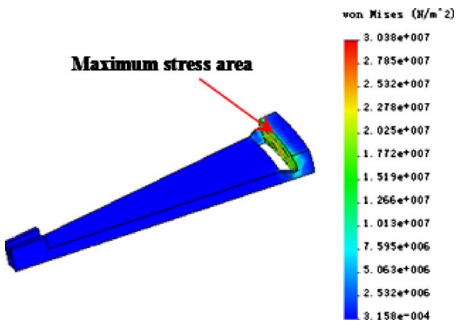

Fig. 8 Thermal stress distribution of wafer 3

Downloaded From: http://asmedigitalcollection.asme.org/ on 10/11/2015 Terms of Use: http://www.asme.org/about-asme/terms-of-use

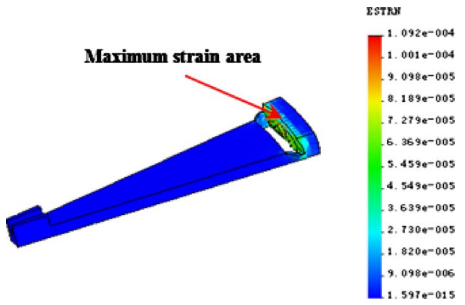

Fig. 9 Thermal strain distribution of wafer 3

bonded position between the tail of wafer 4 and wafers 1, 2, and 3 (see the yellow arrowhead in Fig. 10). The FEM analysis focused on the tail of wafer 4 (see Fig. 10(*c*)).

From Fig. 11, the maximum stress and strain also occur at the interface of wafers 3 and 4, i.e., the outer fringe of the junction. The calculated results reveal that the distortion due to high temperature occurs at the bonded locations. Therefore, it is considered that the high thermal stress and strain may further aggravate the deleterious effects of bow and warpage from the fabrication process, making the protrusions on the surface of the fourth wafer larger than before (see Fig. 5). Consequently, this may significantly decrease the bonding strength in the fifth wafer, causing the combustor failure (Fig. 12).

In order to further verify the deleterious effect from wafers 1,2, and 3, wafers 4 and 5, the interfaces of the other wafers in the combustor, e.g., the interface between wafers 3 and 4 and between wafers 5 and 6, were also calculated using the FEA method. The results are illustrated in Fig. 13, where distance denotes the length measured from the inner wall toward the outer wall (see Fig. 10(*c*)). The distance simulated is up to 0.5 mm. From Fig. 13, it

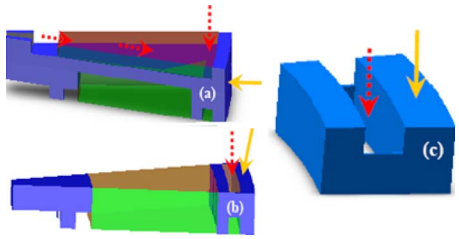

Fig. 10 Schematic of (*a*) wafers 3 and 4, (*b*) of wafer 4, and (*c*) the tail of wafer 4

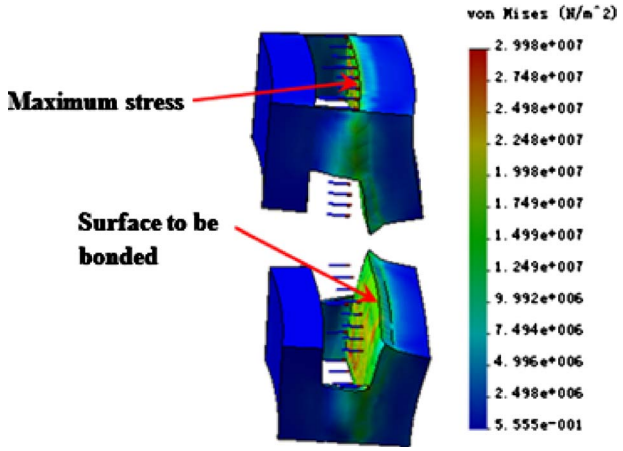

Fig. 11 Thermal stress distribution on the tail of wafer 4

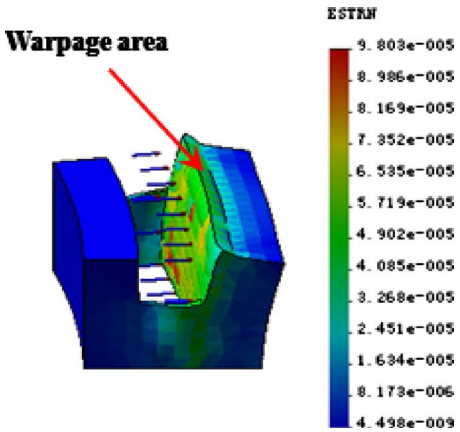

Fig. 12 Thermal strain distribution on the tail of wafer 4

could be inferred that the thermal stresses on either wafers 1, 2, and 3 or wafers 4 and 5 are much higher than those on either wafers 3 and 4 or wafers 5 and 6.

Although the peak thermal stresses obtained are small for a lower temperature, at the current level of temperature (>1200 K), they are comparable to the available strength (~50 MPa), as depicted above. Additionally, the residual stresses in the fabrication process of the microcombustor are neglected due to the insufficient data related, but they may have deleterious effects on the microcombustor [15,16]. Consequently, under the combinational effects of the congregated stress, the poor bonding, the high thermal stress, and the residual stresses, the bonding junctions of wafers 1, 2, and 3 and wafers 4 and 5 could be weakened, and therefore result in fatigue failure.

5 Conclusions

The 2D CFD based numerical simulation results show that the flame could cause the combustor wall temperature to be higher than the auto ignition temperature of reactants, possibly damaging the device when the heat transfer coefficient is sufficiently low. Optimizing the heat transfer coefficient on the outer wall is therefore the most effective approach to manage the combustor wall temperature.

For a silicon microcombustor, the thermal stress may be a significant design restriction in the stationary structure due to the

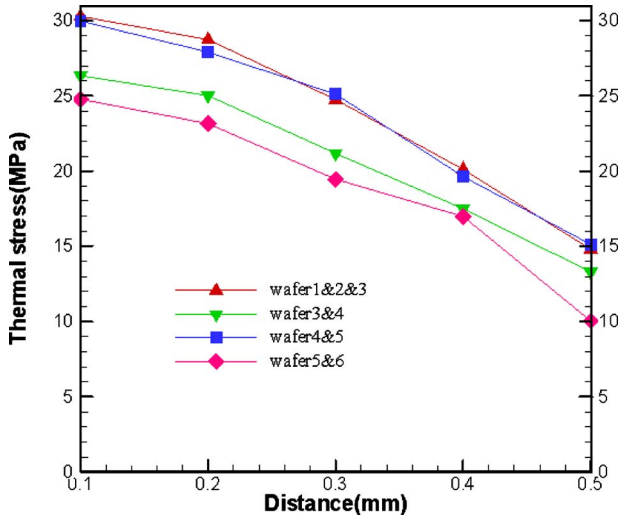

Fig. 13 Thermal stress distribution on the interfaces of other wafers

Downloaded From: http://asmedigitalcollection.asme.org/ on 10/11/2015 Terms of Use: http://www.asme.org/about-asme/terms-of-use

higher temperature (and lower strength). The calculated results in this study indicate that the thermal stress due to sufficiently high temperature may weaken the bonding strength and accelerate the failure of the combustor.

Acknowledgment

L.Z. would like to thank the financial support for the project from the Chinese National Foundation (Grant No. 50721140651) and Anhui Province National Foundation (Grant No. KJ2009B004Z). T.-C.J. would also like to acknowledge the partial financial support from EPA (Grant No. RD833357).

Nomenclature

C_p = specific heat, J/kg K
EX = elastic modulus, Pa
K = conductivity, W/m K
T = ambient temperature, K
μ = Poisson's ratio
σ_s = yield strength, MPa
ρ = density, kg/m^3
h = heat transfer coefficient on the outer wall, W/m^2 K
V = mass flow rate of the mixture, g/s
ε = radiation emissivity of silicon
δ = equivalence ratios of the hydrogen/air mixture
α = coefficient of thermal expansion of silicon

References

[1] Epstein, A. H., 2003, "Millimeter-Scale, MEMS Gas Turbine Engines," Proceedings of ASME Turbo Expo 2003 Power for Land, Sea, and Air, Atlanta, GA, pp. 16–19.
[2] Hua, J., Wu, M., and Kumar, K., 2005, "Numerical Simulation of the Combustion of Hydrogen-Air Mixture in Micro-Scaled Chambers Part II: CFD Analysis for a Micro-Combustor," Chem. Eng. Sci., **60**, pp. 3507–3515.
[3] Mehra, A., 2000, "Development of a High Power Density Combustion System for a Silicon Micro Gas Turbine Engine," Ph.D. thesis, Massachusetts Institute of Technology, Cambridge, MA.
[4] Spadaccini, C. M., 2004, "Combustion Systems for Power-MEMS Applications," Ph.D. thesis, Massachusetts Institute of Technology, Cambridge, MA.
[5] Spadaccini, C. M., Lee, J., and Zhang, X., 2003, "High Power Density Silicon Combustion System for Micro Gas Turbine Engines," ASME J. Eng. Gas Turbines Power, **125**, pp. 709–719.
[6] Mehra, A., and Waitz, I. A., 1998, "Development of a Hydrogen Combustor for a Microfabricated Gas Turbine Engine," Solid State Sensor and Actuator Workshop, Hilton Head Island, SC, pp. 224–231.
[7] Chen, K. S., 1999, "Materials Characterization and Structural Design of Ceramic Micro Turbo Machinery," Ph.D. thesis, Massachusetts Institute of Technology, Cambridge, MA.
[8] Hua, J., Wu, M., and Kumar, K., 2005, "Numerical Simulation of the Combustion of Hydrogen-Air Mixture in Micro-Scaled Chambers. Part I: Fundamental Study," Chem. Eng. Sci., **60**, pp. 3497–3506.
[9] Bagdahn, J., Sharpe, W. N., Jr., and Jadaan, O., 2003, "Fracture Strength of Polysilicon at Stress Concentrations," J. Microelectromech. Syst., **12**(3), pp. 302–312.
[10] Miki, N., Zhang, X., Khanna, R., Ayón, A. A., Ward, D., and Spearing, S. M., 2003, "Multi-Stack Silicon-Direct Wafer Bonding for 3D MEMS Manufacturing," Sens. Actuators, A, **103**, pp. 194–201.
[11] Mehra, A., Arturo, A., Ayon, I., Waitz, A., and Schmidt, M. A., 1999, "Microfabrication of High Temperature Silicon Devices Using Wafer Bonding and Deep Reactive Ion Etching," J. Microelectromech. Syst., **8**(2), pp. 152–160.
[12] Chen, K.-S., Ayon, A. A., Zhang, X., and Spearing, S. M., 2002, "Effect of Process Parameters on the Surface Morphology and Mechanical Performance of Silicon Structures After Deep Reactive Ion Etching," J. Microelectromech. Syst., **11**(3), pp. 264–275.
[13] Klaassen, E. H., Petersen, K., Noworolskil, J. M., Logan, J., Maluf, N. I., Brown, J., Storment, C., McCulley, W., and Kovacs, G. T. A., 1996, "Silicon Fusion Bonding and Deep Reactive Ion Etching: A New Technology for Microstructures," Sens. Actuators, A, **52**, pp. 132–139.
[14] Park, J., and Choi, H. C., 2005, "FEM Analysis of Multilayered MEMS Device Under Thermal and Residual Stress," J. Microsystem Technology., **11**, pp. 925–932.
[15] Zhang, X., Ghodssi, R., and Chen, K. S., 2000, "Residual Stress Characterization of Thick PECVD TEOS Film for Power MEMS Applications," Solid-State Sensor and Actuator Workshop, Hilton Head Island, SC, pp. 316–319.
[16] Zhang, X., and Chen, K. S., 2002, "Residual Stress and Fracture of Thick Dielectric Films for Power MEMS Applications," The Fifteenth IEEE International Conference on Micro Electro Mechanical Systems, Las Vegas, pp. 164–167.

Downloaded From: http://asmedigitalcollection.asme.org/ on 10/11/2015 Terms of Use: http://www.asme.org/about-asme/terms-of-use